available at www.sciencedirect.com

ScienceDirect

journal homepage: www.elsevier.com/locate/ecolmodel

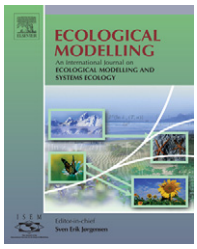

Soil water carrying capacity for vegetation: A hydrologic and biogeochemical process model solution

Y.Q. Xia [a,b], M.A. Shao [c,*]

[a] Key Laboratory of Land Water Cycle and Related Land Surface Processes, Institute of Geographical Sciences and Natural Resources Research, Chinese Academy of Sciences, Beijing 100101, China

[b] Graduate School of the Chinese Academy of Sciences, Beijing 100039, China

[c] Institute of Soil and Water Conservation, Chinese Academy of Sciences & Ministry Water Resource, Northwest A&F University, Yangling 712100, China

ARTICLE INFO

Article history:
Received 1 November 2006
Received in revised form
30 December 2007
Accepted 29 January 2008
Published on line 25 March 2008

Keywords:
Hydrologic cycle
Biogeochemical processes
Soil water carrying capacity
Arid and semi-arid area
Vegetation density
Model

ABSTRACT

The research for a maximum stand density that maintains sustainable development is necessary in arid and semi-arid areas where the conflict between limited soil water storage and the need for more plants in improving environmental quality almost always exists. However, the quantification of the research is not easy since it requires insight interpretations of the effects of plant density on soil water storage and soil water stress on plant growth. Such quantification is incomplete with current empirical methods or physical models because the dynamics effects of soil water stress and its feedbacks are not included. This paper presents a physically based model of soil water carrying capacity for vegetation (SWCCV). The model build on the concept of an equilibrium adjustment of vegetation growth to soil water dynamics, by iterative calculation between hydrologic and biogeochemical processes that account for the interactions between the limiting effects of soil moisture on photosynthesis and evaporative demand on soil water. It is capable to calculate the maximum plant density at any given initial conditions (site-specific data, vegetation, weather, and etc.) through hourly, daily and yearly cycles. Exploratory simulation to evaluate the model against results from previous studies for two sites indicated that the predictions by the model had good agreement with measured soil water contents in each layer, LAI and NPP for plants. Under the same initial conditions the predicted soil water carrying capacity captured well the soil water difference between two sites in terms of controlling vegetation density. Overall, the SWCCV model is capable in terms of predicting soil water carrying capacity, providing a new approach for understanding soil–vegetation interactions and making recommendations for better management of vegetation construction in arid and semi-arid areas.

1. Introduction

Deep insight understanding the relationship between soil water dynamics and vegetation density is helpful for making recommendations to soil erosion control and vegetation construction in semi-arid and arid areas (Braud et al., 2001; Yu et al., 2006; Zhou et al., 2006). On one hand, increasing vegetation density can significantly reduce sediment yield because of rapidly increasing land coverage, and resulting in an effective control of soil erosion (Bosch and Hewlett, 1982; Gardiol et al.,

* *Corresponding author*. Tel.: +86 29 87012405; fax: +86 29 87012334.
E-mail address: mashao@ms.iswc.ac.cn (M.A. Shao).

0304-3800/$ – see front matter © 2008 Published by Elsevier B.V.
doi:10.1016/j.ecolmodel.2008.01.024

2003; Khanna et al., 1999; van Dijk and Bruijnzeel, 2003; Wang and Cai, 1999; Yu et al., 2006; Zhou et al., 2006). On the other hand, soil water should be prevented from excessive consume by vegetation since an increase in plant cover increases evapotranspiration (Kyushik et al., 2005). Soil water is the limiting factor in determining the vegetation density in the arid and semi-arid areas. Thus, the search for a maximum stand density as a basis for sustainable development is necessary in the areas where the conflict between limited soil water and much of required plant almost always exists.

The underlying concept and premises of carrying capacity, employed as tools for the operationalization of sustainable development (Schneider et al., 1978), is a very ambiguous term in ecology. It usually means to be the maximum number of individuals that can be supported in an environment without the area experiencing decreases in the ability to support future generations within that area (Guo and Shao, 2004). Moreover, planners usually define carrying capacity as the ability of a natural or artificial system to support the demands of current and future development without considerable degradation or damage (Zeide, 2004). Concern over rising planting in arid and semi-arid regions, and accompanying impacts on soil water, led the management to focus increasing attention on the concept of soil water carrying capacity (Guo and Shao, 2004). In particular, the concept may be useful in vegetation and range management as a general definition of carrying capacity does in ecosystem. Here soil water carrying capacity is defined as: a maximum vegetation density that an arid or semi-arid area will support without soil water experiencing decreases in the ability to support future generations during plant growth period, given the desired climatic condition, soil texture, and management program. "The desired climatic condition, soil texture, and management program" recognizes the need to be comprehensive, integrative, concurrent, and holistic in decision making. It is a useful concept for theoretical system modeling, but it is very problematic for practical application. In the real world, virtually no habitat is stable indefinitely. Seasonal variations occur throughout the year even the day; annual variations occur between years (e.g., weather); and disturbances, succession, ecological change are present over both short and long time scales. "Maximum vegetation density" can vary, depending on type and age composition desired or assumed, as well as expectations for biomass of the plant (e.g., "maximum sustained yield").

In practical application, carrying capacity is best determined empirically, after carefully defining exactly what is meant about location, climatic condition, reasonable limits of natural variation (e.g., are droughts or innutrition included?), and physiological characteristics of vegetation. It requires much empirical experience with the vegetation and the site-specific condition. Yet, extrapolation to other location than those specific lands studied involves much uncertainty. As for quantifying optimization vegetation for each position for anytime in catchment, empirical determination of carrying capacity is almost impossible.

Until recently, relatively little work has been done on theoretical calculation or estimation model of carrying capacity for vegetation. Zeide (2004) developed a simple model that accounted for each main growth predictor individually which allows one to calculate the density that maximizes volume growth at a given time. However, in the model soil moisture is not modified by plant density and does not restrict plant growth. Thus, the model is not in tune with the water and heat transfer character of soil-plant-atmosphere continuum. Based on the interaction between soil water supply and planting density, the empirical model derived from field trials did not consider soil moisture availability and the processes happened in soil–plant system, therefore, interactions between soil and plant are static and fixed, and consequently the model is difficult to model or predict (Guo and Shao, 2004). As these models do not ensure physical consistency of system solutions, Devonec and Barros (2002) has suggested materials process analysis to ensure such a consistency.

Physically based process model, which provide a dynamic way of determining soil water carrying capacity for vegetation, is confounded by two major problems: (1) hydrological and biogeochemical process are not on balance one another, and (2) biomass was used as a parameter inputted into the model by the trial and error method, it is really difficult to obtain the optimization vegetation density. As examples of biogeochemical models, such as FOREST-BGC (Aber and Federer, 1992), BIOME-BGC (Parton et al., 1996), PnET (Farquhar et al., 1980), and CENTURY (Garcia-Quijano and Barros, 2005) utilize variations of a photosynthesis model proposed by Farquhar et al. (Vörösmarty et al., 1989), which calculates CO_2 assimilation as a function of the carboxylation and oxygenation velocities, photosynthetic electron transport and dark respiration. However, moisture availability controls in the atmosphere (water vapor pressure) and soil (soil water content) are not taken into account, and therefore soil water stress to photosynthesis (Parton et al., 1996; Vörösmarty et al., 1989). In spite of the degree of biogeochemical detail present in this model, the physically based hydrological process is described in a relatively simple way, using of empirical formulas which are restricted to specific environment, or the hydrological model is run separately (Devonec and Barros, 2002). Therefore, the predicted soil water dynamics is not accurate because it is not affected by vegetation growth and the feedbacks of evapotranspiration and runoff (Devonec and Barros, 2002; Garcia-Quijano and Barros, 2005). With regard to hydrological models, in which each hydrologic process is described by semi-empirical function based on field data in great detail (Running et al., 1987), but are based on the assumption that the vegetation is static, neglecting feedbacks involving photosynthesis, soil moisture, and transpiration (White et al., 2000). Furthermore, most hydrological models rely on point measurements of LAI and assume that transpiration is uniform within the canopy independent of the height of each foliage layer. In our efforts to understand the interactions between soil water dynamics and vegetation growth, it has been increasingly recognized that hydrological and biogeochemical cycles need to be modeled in details coequally.

In order to take an effective approach to resolve this dilemma, we here present a quantifying model of Soil Water Carrying Capacity for Vegetation (SWCCV) that integrates hydrological and biogeochemical process and to examine the results that are obtained from field data. The model was built

Table 1 – Initial conditions and parameter values required to run SWCCV, using *Caragana* at Shenmu site as an example

Atmospheric	
1. Maximal hourly temperature	Degree
2. Minimum hourly temperature	Degree
3. Mean hourly temperature	Degree
4. Hourly rainfall	mm
5. Mean hourly vapor pressure deficit	Pa
6. Hourly solar radiation	$W m^{-2}$
7. Daily length	s
8. Wind speed	$m s^{-1}$
Vegetation	
1. Yearday to start new growth	105*
2. Yearday to end litterfall	281*
3. Transfer growth period as fraction of growing	0.3
4. Litterfall as fraction of growing season	0.2
5. Annual leaf and fine root turnover fraction	$0.32\ Year^{-1}$
6. Annual live wood turnover fraction	$0.07^{*}\ Year^{-1}$
7. Annual whole-plant mortality fraction	$0.02\ Year^{-1}$
8. New root C:new leaf C	0.78**
9. New stem C:new leaf C	0.22
10. New live wood C:new total wood C	0.1*
11. Current growth proportion	0.5
12. C:N of leaves	$25^{**}\ kg C kg N^{-1}$
13. C:N of leaf litter	$75 kg C kg N^{-1}$
14. C:N of fine roots	$21.79^{**} kg C kg N^{-1}$
15. Leaf litter labile proportion	0.2876**
16. Leaf litter cellulose proportion	0.5124**
17. Leaf litter lignin proportion	0.19**
18. Maximum wiltdays vegetation can suffer (n)	20* days
19. Fine root labile proportion	0.34
20. Fine root cellulose proportion	0.44
21. Fine root lignin proportion	0.22
22. Canopy water interception coefficient	0.1*
23. Canopy light extinction coefficient	$0.55 LAI^{-1} d^{-1}$
24. All-sided to projected leaf area ratio	2.3
25. Canopy average specific leaf area	$34.1^{*} m^2 kg C^{-1}$
26. Ratio of shaded SLA:sunlit SLA	2
27. Fraction of leaf N in Rubisco	0.04
28. Cuticular conductance	$0.00006 m s^{-1}$
29. Effective root proportion in each soil layer	–
30. Leaf width	0.02*m
31. Height of canopy	1.6* m
Site	
1. Elevation	1094 m
2. Latitude	38.5 decimal degrees
3. Longitude	110.3 decimal degrees
4. Site shortwave albedo	0.2
5. The height of the reference	2 m
6. Atmospheric CO_2	387 ppm
7. Starting biomass	$t ha^{-1}$
Soil	
1. Soil texture	sand, silt, and clay percent
2. Starting soil moisture	$m^3 m^{-3}$
3. Depth of each soil layer	m
4. Wilt point	$0.04 m^3 m^{-3}$
5. Soil density	$1.45 g cm^{-3}$
6. Soil N	$kgN m^{-2}$
7. Soil C	$kgC m^{-2}$

For vegetation parameters, Values with (*) are measured at the Shenmu site, values with (**) are from literature (Xu et al., 2001), and other values are from literature (White et al., 2000).

and validated currently at Shenmu site in the north of the Loess Plateau, China. It was hypothesized there were no irrigation conditions and the ground water was too deep to uptake by vegetation root. The model was construct on the concept of the equilibrium adjustment of vegetation growth to soil water deficits, by iterative calculation between hydrologic and biogeochemical process that accounts for the interactions between the limiting effects of soil moisture on photosynthesis and evaporative. It attempts to account for not only carbon assimilation and nutrient cycling, but also soil water dynamics, as well as feedbacks between soil hydrology and vegetation processes. Therefore, this model is capable to calculate the dynamic maximum plant density at any given initial conditions (site-specific data, vegetation, weather, and etc.).

2. Model development

2.1. Algorithm

The model is driven by hourly meteorological data normally available from routine sources (Table 1), although vapor pressure deficit and solar radiation can be derived from climatological principles (Running et al., 1987). Typically, the vegetation is characterized by its physiological and physical properties proposed by Chen et al. (1999). Site-specific data and vegetation physiological parameters (Table 1) are initialized at the beginning of simulation, and then soil moisture is used as a primary diagnostic for LAI and vegetation growth simulation. For each daily step, the hydrological equilibrium is determined by LAI and soil water stress that occur during the leaf-on season. Drought tolerance strategy is accounted for by allowing an n-day period during which soil water content can be less than wilting point. The values of LAI_a and LAI_b ($LAI_b > LAI_a$) are initialized as 0 and the double value of LAI_0, respectively. At the running of the model, the value of LAI is equal to the average value of LAI_a and LAI_b. The value of LAI_b is set to the calculated value of LAI when the successive number of wilting days (n_{sw}) is great than n in daily step, and LAI_a is unchanged, if so, the cycle is reset (Fig. 1). Wilting point is defined as the inextractable soil water by vegetation, which is mainly characterized by soil texture and vegetation type. On the other hand, the value of LAI_a is set to the calculated value of LAI when soil water is never below wilting point during plant growing period in yearly step, and LAI_b is unchanged, then the cycle is also reset. The process stops when the number of wilting days is less than the maximum days vegetation can suffer ($n_{sw} < n$). So, starting from values of vegetation parameters and site-specific data, which represent current environmental setting, we can successively appraise whether the current vegetation density is favorable or not. In general, we can acquire good results within 10 cycles. By this means of iterative calculation between hydrologic and biogeochemical processes, the iterative process stops when the maximal vegetation density or biomass is obtained without soil water content being less than the wilting point. As detailed hereafter, particular attention has been paid to processes which influence (either strengthen or weaken) the relationship between the production of vegetation and soil water.

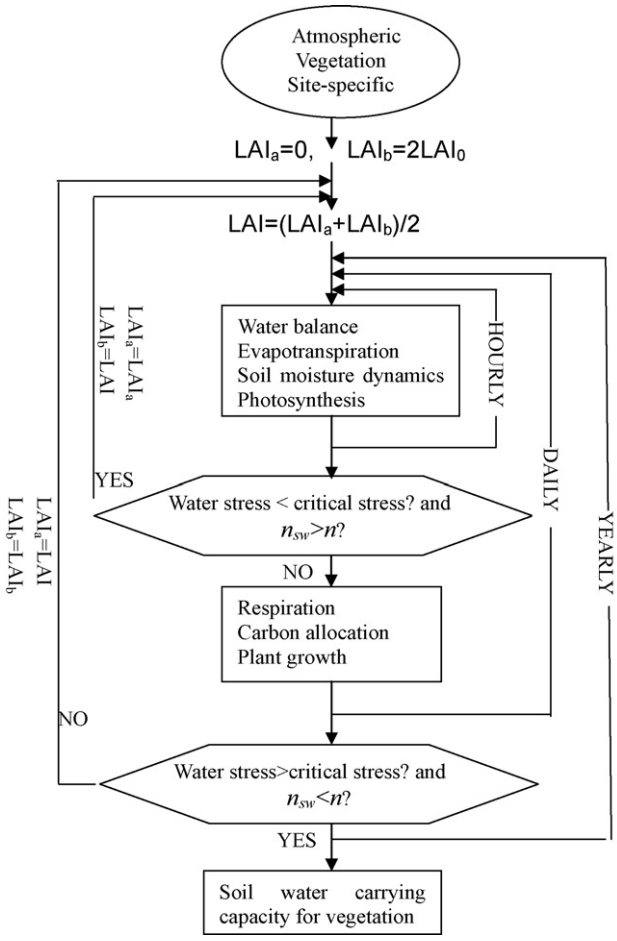

Fig. 1 – Algorithm for SWCCV. LAI_0 is derived from current vegetation attributes. The value of LAI is set equal to the average value of LAI_a and LAI_b with the initial value of 0 and 2 LAI_0, respectively. LAI_b is set to the calculated value of LAI when the number of days for soil water below wilting point (n_{sw}) is great than vegetation can suffer (n) in daily cycles, and LAI_a is unchanged. Whereas the value of LAI_a is set to LAI as soil water is never below wilting point during plant growing period in yearly cycles, and LAI_b is unchanged. The process stops when the maximal vegetation production is obtained with the number of wilting days less than the maximum days vegetation can suffer ($n_{sw} < n$).

2.2. Model description

The modeling approach consists of a hydrological model and a biogeochemical model based on the assumption that soil water carrying capacity is primary a function of climate and general life-form characteristics. For this model component, many authors have introduced detailed formulae describing the corresponding process and parameters. In this section, we focus mainly on describing the essential framework as well as the interactions between hydrological controls and vegetation processes introduced in the context of this work.

2.2.1. *Radiative transfer*

The SWCCV model surface radiation through a series of canopy layers which correspond to overstory and understory vegetation. The canopy energy balance (R_n) is described by:

$$R_n = \lambda E + H + G \quad (1)$$

where λE is the total latent radiation comprising latent radiation for transpiration and soil evaporation, H is the sensible heat flux, and G is the ground heat flux.

Canopy radiation interception depends upon top of canopy inputs of both diffuse and direct solar radiation and direct solar radiation as well as longwave radiation. Within SWCCV, these radiation streams are input by the user (Table 1) and then adjusted to account for atmospheric transmissivity, estimated based on hourly temperature variation and precipitation. These equations are not described here since they mainly follow the MTN-CLIM approaches (Monteith, 1965), but the day-step is modified to hour-step. Canopy radiation attenuation and absorption by each canopy layer is modeled separately for shortwave and photosynthetically active radiation (PAR) radiative fluxes.

Field evidence has shown that sunlit and shaded leaves respond differently in terms of photosynthetic efficiency, leaf nitrogen content, and specific leaf area. To account for this, we partition the canopy into sunlit and shaded components (Shuttleworth and Wallace, 1985). The total shortwave absorbed by sunlit and shaded canopy fractions (Sw_{sun} and Sw_{shade}, respectively) is based on Beer's law such that:

$$Sw_{sun} = Sw_c \times \alpha \times LAI_{sun} \quad (2)$$

$$Sw_{shade} = Sw_s - Sw_{sun} \quad (3)$$

where Sw_c is the shortwave to upon top of canopy stratum, Sw_s is the shortwave to soil surface stratum, α is the canopy light extinction coefficient, and LAI_{sun} is the projected LAI for sunlit portions.

Absorbed PAR (PAR_{sun}; PAR_{shade}) are calculated using Eqs. (2) and (3) above where Sw_c, Sw_s and α are replaced by the PAR to upon top of canopy stratum and the PAR to soil surface stratum, and PAR-specific coefficients.

2.2.2. *Hydrological process*

The conception model of water balance can be expressed as the sum of precipitation Pr and snow melt S^{melt} is equal to evapotranspiration ET_a, soil water infiltration f_t, drainage runoff R_{off}, and canopy interception losses I_t:

$$Pr + S^{melt} = ET_a + R_{off} + f_t + I_t \quad (4)$$

2.2.2.1. *Interception losses*. Rainfalls are intercepted by the canopy and are evaporated at the potential rate. Interception of incoming rainfall by vegetation can amount to more than 10% of the annual rainfall and therefore affect the soil moisture availability. In arid and semi-arid region where most of the rainfall occurs in low frequency, the effect of canopy interception on the soil water balance cannot be ignored. Interception generally increases along with the LAI. Here, interception is a function of the water-holding capacity of the vegetation and considered to be proportional to LAI and to the incoming precipitation:

$$I_t = \min(\beta \times LAI \times Pr, I_{t\,max} - \theta) \quad (5)$$

where the coefficient β is water interception coefficient and is a proxy for the rainfall regimes effect, I_{tmax} is the current time maximum interception storage, and θ is the initial canopy water storage. For an LAI of 2, interception is than 10% of incoming rainfall for an arid shrub.

2.2.2.2. *Evapotranspiration*. Total evaporative fluxes from each canopy layer may include the evaporation of water intercepted by the canopy, sublimation of intercepted snow, and transpiration by vascular layers. The Penman–Monteith (Shuttleworth and Wallace, 1985) equation is based on the single source-sink assumption, which does not apply to sparse vegetation, Shuttleworth and Wallance (Laio et al., 2001; Schulze, 1986) extended the P-M method to two surface: the canopy and the soil. In their model, total ET is expressed as:

$$\lambda ET = C_c ET_c + C_s ET_s \quad (6)$$

where λET is the sum of the latent heat flux from canopy and soil (MJ m^{-2}), λ is the latent heat of water vaporization (MJ kg^{-1}), ET_c and ET_s are canopy transpiration and soil evaporation (MJ m^{-2}), respectively, C_c and C_s are weighting coefficients expressed as function of resistance, whose complete formulation is given by Shuttleworth and Wallance (Gifford, 1976). The ET_c and ET_s terms have the following form:

$$ET_c = \frac{\Delta(R_n - G) + [\rho_a C_p D - \Delta r_{ac}(R_{ns} - G)]/(r_a + r_{ac})}{\Delta + \gamma(1 + (r_c/(r_a + r_{ac})))} \quad (7)$$

$$ET_s = \frac{\Delta(R_n - G) + [\rho_a C_p D - \Delta r_{as}(R_n - R_{ns})]/(r_a + r_{as})}{\Delta + \gamma(1 + (r_s/(r_a + r_{as})))} \quad (8)$$

where Δ is the slope of saturation at constant pressure (kg m^{-3}), R_n is the net radiations above canopy (MJ m^{-2}), R_{ns} is the net radiation above soil surface (MJ m^{-2}), ρ_a is the mean air density at constant pressure (kg m^{-3}), G is the soil heat flux (MJ m^{-2}), C_p is the specific heat of moist air at constant pressure (kg m^{-3}), γ is the phychrometric constant (kPa °C^{-1}), r_a is the aerodynamic resistance (m s^{-1}), r_c is the canopy resistance (m s^{-1}), r_s is the soil resistance (m s^{-1}), r_{ac} and r_{as} are the aerodynamic resistance from soil to canopy and from canopy to reference height (m s^{-1}), respectively.

Much of the remainder of the model involves calculating the limiting resistances (r_a, r_c, r_{ac}, r_s and r_{as}) of evaporation and transpiration.

As long as soil moisture is sufficient to permit the normal course of plant physiological processes, evapotranspiration is assumed to occur at a potential rate PET, which is independent of θ. However, when soil moisture falls below a given point θ^*, which, as we shall see, depends on both vegetation and soil characteristics, plant start reducing transpiration closing their stomata to prevent internal water losses (Maidment, 1993). Below θ^*, soil water availability becomes a key factor in determining the actual evapotranspiration. Photosynthesis-related transpiration and root water uptake continue at a reduced rate

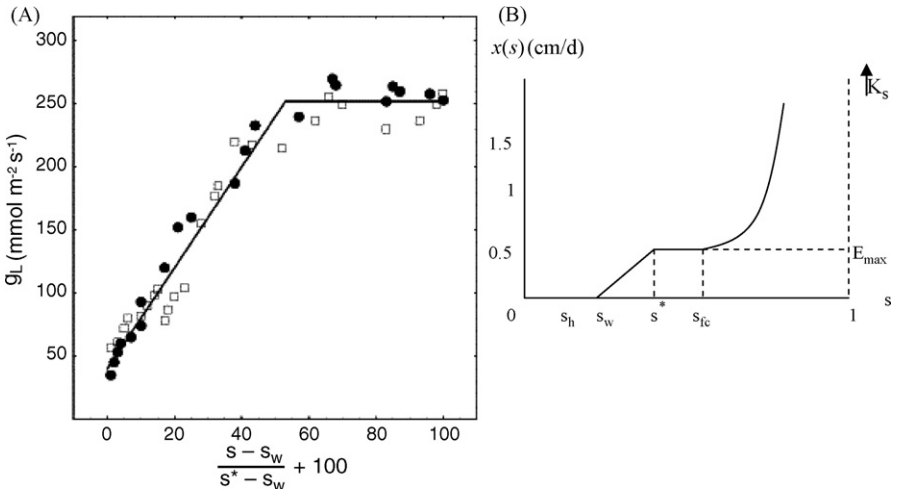

Fig. 2 – (A) Leaf conductance g_L vs. soil moisture level for *Nerium oleander*, measured maintaining two different levels of vapor pressure deficit (soil circles and open squares, respectively) (adapted from (Schulze, 1986)). (B) Behavior of soil water losses (evapotranspiration), *x*(*s*), as function of relative soil moisture for typical climate, soil and vegetation characteristics in semi-arid ecosystems (Laio et al., 2001).

until soil moisture reaches the wilting point θ_w. The relationship between the rate of plant water uptake and soil moisture content between θ^* and θ_w is well approximated by a linear decrease. Fig. 2A shows an example of the relationship between leaf conductance and soil moisture content measured during a controlled experiment. The strongly nonlinear, threshold-like dependence of the transpiration rate on soil moisture is clearly evident. The dependence of evapotranspiration losses on soil moisture is summarized in the following expression:

$$f(\theta) = \begin{cases} 1 & \theta \geq \theta^* \\ \dfrac{\theta - \theta_w}{\theta_{fc} - \theta_w} & \theta_w < \theta < \theta^* \\ 0 & \theta \leq \theta_w \end{cases} \quad (9)$$

$$ET_a = PET \times f(\theta) \quad (10)$$

whose behavior is shown in Fig. 2B. The introduction of $f(\theta)$ is necessary to represent better the soil moisture dynamics under drought conditions as well as for the related analysis of crossing properties of the wilting point level.

2.2.2.3. *Soil water, infiltration and surface runoff.* The dynamics of soil moisture is described with a series layers scheme, in which each layer acts as a source of root uptake for canopy transpiration decided by its root length density, beside that the first layer as the source of soil evaporation and the last layer as the drainage layer. We use subscripts *i* for the time, *n* for the number of soil layers, and *j* for the serial number of soil layers ($1 < j < n$). The governing equations are expressed as follows:

$$\frac{\partial \theta_{i,1}}{\partial t} L_{i,1} = S_i^{melt} + f_i + Pr_i - R_{off} - I_{ti} - Gd_{i,1} + \Phi_{diff_{i,2}} - E_i - Ru_{i,1} \quad (11)$$

$$\frac{\partial \theta_{i,j}}{\partial t} L_{i,j} = Gd_{i,j-1} - Gd_{i,j} + \Phi_{diff_{i,j+1}} - \Phi_{diff_{i,j}} - Ru_{i,j} \quad (12)$$

$$\frac{\partial \theta_{i,n}}{\partial t} L_{i,n} = Gd_{i,n-1} - \Phi_{diff_{i,n}} \quad (13)$$

where R_{off} is overland runoff water (mm), E is soil evaporation (mm), L is the thickness of the soil layer (m), θ is the soil moisture in the soil layer ($cm^3\,cm^{-3}$), f_i is soil water infiltration (mm), Φ_{diff} is the flow between the soil layers (mm), Ru is the root uptake soil water (mm), and Gd is the gravitational drainage from the soil layer (mm).

The model was run with an hourly time step with climate data because of high frequency and intensity storm in semi-arid and arid environment and it affect the soil water balance immediately. For the *j*th layer it is assumed that macropore flow does not allow water to move into the layer below until θ_{fc} is reached. The amount of through flow is based on an estimate of the field capacity of the soil water storage at which through flow begins and an estimate of the rate of through flow.

Simplified and suitable approaches are usually required for describing local infiltration in rainfall-runoff models designed for practical applications. Gifford (Tague and Band, 2004) examined the suitability of the Horton, Kostiakov and Philip models for infiltration data collected from a variety of mostly semi-arid rangeland plant communities from both Australia and the USA. Nearly 1100 infiltrometer plots were included in the analysis. His results indicated that the Horton model best fit the infiltrometer data.

$$f_t = f_c + (f_0 - f_c)e^{-kt} \quad (14)$$

where f_c is the steady state value of infiltration ($mm\,h^{-1}$), f_0 is the initial state value of infiltration ($mm\,h^{-1}$), and k is the infiltration decay factor (min^{-1}).

Eq. (14) is derived from the simple assumption that the reduction in infiltration capacity during rain is directly pro-

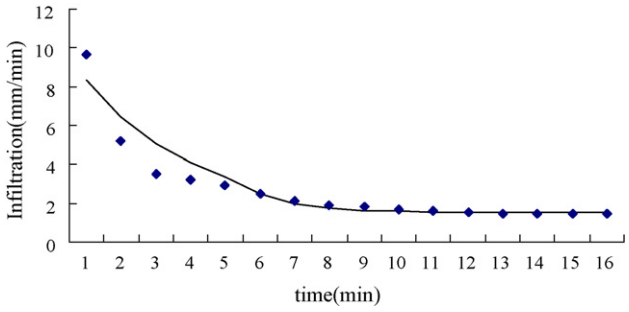

Fig. 3 – Using field data (symbols) to fit Horton model empirical parameters by straight-line fitting method.

portional to the rate of infiltration and is applicable only when the effective rainfall intensity is great than f_c. Maidment (Molz and Remson, 1970) provide generalized estimates of f_0 varying from 210 to 900 mm h^{-1}, f_c from 2 to 290 mm h^{-1}, and k from 0.8 to 2.0 min^{-1} for soils ranging from fine sandy clay to standard turfed agricultural soil. For field applications, the model parameters are usually estimated by empirical fitting (Fig. 3).

Therefore, the amount of run-off is influenced by storm size, storm intensity, slop, vegetation cover, soil type, and soil surface condition. Run-off is difficult to estimate without considerable site-specific data. In SWCCV we use the value of the effective rainfall intensity minus f_t for run-off, which has yielded satisfactory results for most of sites used in estimating the amount of the run-off and has the advantage that it involves no extra site-specific estimates.

2.2.2.4. *Snow melt*. For arid and semi-arid regions, the snow melt is an important water resource. Snowmelt, S^{melt}, is computed using a quasi-energy budget approach that takes into account radiation (M_{rad}), a combination of melt due to sensible and latent heat flux (M_T), and advective (M_V) (from rain on snow) controls on snowmelt such that, at a daily time step

$$S^{melt} = M_{rad} + M_T + M_V \tag{15}$$

Melt from temperature and advection occurs only when the snowpack is ripe. Snowpack temperature is approximated using an air temperature accumulation of a snowpack energy deficit (SED):

$$SED_t = \max[SED_{(t-1)} + T_{air}, SED_{max}] \tag{16}$$

where $SED_{(t-1)}$ is the previous day's energy deficit, T_{air} is mean daily temperature, and SED_{max} is a maximum energy deficit that is set as a climate-region-specific input parameter. Melt due to radiation can occur as sublimation when the energy deficit SED is less than 0 (Jamieson and Ewert, 1999; Li et al., 2001). This scheme aims at simulating snow dynamics more sophisticatedly, and more physically sound schemes can be used in cases where the focus is on snow physical processes.

2.2.2.5. *Water uptake by roots*. Root water uptake is time and space dependent and is governed by soil properties, vegetation characteristics and weather conditions. There are two different approaches to quantify root water uptake: the microscopic and the macroscopic one. The microscopic approach considers that radial flow of soil water toward and into a representative individual root can be represented by infinitely long cylinder of uniform radius and water absorbing properties, which is currently not practical. The more empirical macroscopic approach deals with the removal of water from the root zone as a whole, without considering explicitly the effects of individual roots, and is generally favored in management-oriented soil water simulation models.

Farquhar et al. (1980) assumed that water uptake $R'_u(z, t)$ can be described as a function of transpiration rate, $T(t)$ and a so-called "effective root distribution" function $L_e(z,t)$

$$R'_u(z, t) = \frac{T(t)L_e(z, t)D(\theta)}{\int_0^{z_r} L_e(z, t)D(\theta)dz} \tag{17}$$

where t is the time, z is the soil depth, z_r is the root depth, and $D(\theta)$ is the soil water diffusivity.

Various authors have considered the fact that the root-water uptake was limited by water stress (Ryan, 1991). We assumed a linear decrease in water uptake with soil water stress resistance $R_w(z)$

$$R_w(z) = \frac{f(\theta, z)}{\int_0^{z_r} f(\theta, z)dz} \tag{18}$$

$$R_u(z, t) = R'_u(z, t) \times R_w(z) \tag{19}$$

where $f(\theta,z)$ is a function of soil water resistance in soil depth z (Eq. (9)).

2.2.3. *Carbon and nitrogen cycling*

The carbon and nitrogen balance portion of SWCCV utilizes daily meteorological data and vegetation physiological parameters in conjunction with general stand and soil information to predict net photosynthesis, growth, maintenance and heterotrophic respiration at a daily time-step.

Carbon and nitrogen cycling associated with live vegetation (e.g., photosynthesis, respiration) and hydrologic process is included in canopy strata object routines. Carbon and nitrogen cycling associated with litter and soil layers (e.g., decomposition) occur within patch objects. Thus, all vegetation strata associated with a particular patch contribute and extract material (carbon, water, and nitrogen) to and from the same well-mixed soil and litter pools.

In SWCCV, the C:N ratios of various plant biomass components are fixed based on species-specific input parameters followed with the BIOME-BGC approach and hold leaf and other C:N ratios constant. Within the simulation, however, carbon and nitrogen stores and fluxes are maintained separately to facilitate future implementation of algorithms to account for differences in C:N ratios in response to stress.

2.2.3.1. *Photosynthesis*. The model assumes that photosynthesis is not affected by leaf water status until low relative water content is reached. Photosynthesis was modeled with a biochemical model described by Farquhar et al. (Running and Gower, 1991) that defines the rate of CO_2 fixation from limits of either carboxylating enzyme ribulose bisphosphate caraboxylase (RuBisCO) or the substrate ribulose bisphosphate (RuBP)

which is limited by enzymes (i.e., nitrogen), electron transport (i.e., light), and stomatal conductance (i.e., light and water).

The interactions between soil water, transpiration and carbon assimilation during photosynthesis are accomplished via the relationship between a reduction of plant water potential and plant physiology, which modulates the leaf water potential that regulates carbon assimilation Al at the leaf level. Here, we use a function of water stress to constrain photosynthesis

$$Al(t) = f(\theta) \times A(t) \tag{20}$$

where $A(t)$ is carbon assimilation when there is no water stress, $f(\theta)$ is computed using Eq. (9).

By separately integrating the sunlit and shaded leaf fractions of canopy, a single layered sun/shade model is used, which is as accurate and simple. To account for nonlinearities in the response of sunlit and shaded leaves, assimilation rates are computed separately so that total gross daily canopy photosynthesis, g_{psn}, for the strata becomes

$$g_{psn} = (Al_{sunlit}LAI_{sunlit} + Al_{shaded}LAI_{shaded})D_{len} \tag{21}$$

where subscript sunlit and shaded are sunlit and shaded leaves fraction, separately, Al is carbon assimilation rate, and D_{len} is day length.

2.2.3.2. *Respiration*. Heterotrophic respiration and autotrophic respiration are calculated separately for each part of the plant. Autotrophic respiration is the sum of local growth respiration and maintenance respiration in SWCCV for each component including leaves, roots, and stems, in which maintenance respiration is computed as a function of nitrogen concentration and the current air temperature using the model developed by Ryan (Raich et al., 1991), and growth respiration is computed and subtracted from the carbon allocated to each vegetation component as a fixed percentage of new carbon allocation.

2.2.3.3. *Allocation*. The main structure of allocation in SWCCV is based on BIOME-BGC that photosynthesis is partitioned between roots, stems, and leaves or in case of grasses, between roots and leaves with a fixed partitioning strategy, although many of the specific algorithms have been extended and/or modified.

Plant carbon allocation was modeled based on water and nitrogen limits that influence the overall growth habit of vegetation, represented by shoot v. root allocation, and the amount carbon placed in a plant organ, such as leaf expansion (Lloyd and Taylor, 1994). First, an initial, maximum shoot to root ratio [(shoot/(shoot + root))] was modified by scalar values representing the relative availability of water and nitrogen for leaf growth. The fraction of the new assimilate that is allocated to roots depends on the ratio of actual to potential photosynthesis such that more carbon is allocated to roots when water or nutrient limitations reduce actual photosynthesis. The fraction allocated to roots f_{root}, is computed as

$$f_{root} = \frac{0.8}{1 + 2.5[(psn_{pot}/psn_{actual})]} \tag{22}$$

where psn_{pot} and psn_{actual} are potential photosynthesis and actual photosynthesis in water stress, respectively.

Once the fraction allocated to roots has been determined, the remaining assimilate is allocated to leaves and, in the case of trees, stem wood based on a fixed ratio.

Nitrogen limits were calculated by estimating the amount of leaf nitrogen (N_{leaf}) required to meet a minimum leaf nitrogen concentration as established by the previous years leaf nitrogen content set by the amount of nitrogen available to the plant through uptake (N_{up}) and retranslocation (N_{trans}) from older leaves before abscission where:

$$I_N = \frac{N_{trans} + N_{up}}{N_{leaf}^{t-1}} \tag{23}$$

Nitrogen limitation (I_N) was not allowed to exceed 1.0 once leaf nitrogen demand was satisfied. Available, mineralized nitrogen taken up by plants (N_{up}) was limited by root mass in a Michaelis–Menten function (Andren and Paustian, 1987; Orchard and Cook, 1983).

2.2.3.4. *Mortality*. A daily plant mortality rate as a fixed percentage of current biomass is set in the vegetation physiology parameters file. Total carbon and nitrogen to be lost due to plant mortality is set each day. The same percentage is taken from each of the available tissue stores (i.e., leaves, roots, and stem). Carbon that is lost from leaves and fine roots is transferred to the litter pool. Stem and root material is transferred to a wood debris pool that decays at a species-specific fragmentation rate before it is transferred to litter carbon and nitrogen pools. Fragmentation does not alter wood C:N ratios.

2.2.3.5. *Decomposition*. The nitrogen budget was calculated starting with inputs into the litter. Leaves and fine roots were transformed into litter based on fixed turnover rates. Nitrogen flow into litter was determined from nitrogen in leaves and fine root minus translocation in leaves and a fraction of fine root nitrogen reabsorbed by mycorrhizae. The potential decay rate associated with each soil or litter pool may be reduced as a function of soil moisture and temperature limitations. Scalar multipliers for temperature and moisture effects (t_{scalar} and w_{scalar}, respectively) are computed as follows (Townsend et al., 1995):

$$t_{scalar} = \exp^{308.56[(1/71.02)=1/(T_{soil}+273.15-227.13)]} T_{soil} > -10 \tag{24}$$

$$t_{scalar} = 0.0 T_{soil} <= -10 \tag{25}$$

The soil water potential scalar (w_{scalar}) was calculated based on the logarithmic relationship between soil microbial activity and soil water potential s_p (Ni et al., 2001):

$$w_{scalar} = \begin{cases} 0, & p_{min} > s_p \\ \dfrac{\log(p_{min}/s_p)}{\log(p_{min}/p_{max})}, & p_{min} \le s_p \le p_{max} \\ 1, & s_p > p_{max} \end{cases} \tag{26}$$

where p_{min} and p_{max} are the minimum value of for which soil microbial activity could occur and the maximum soil water potential, respectively.

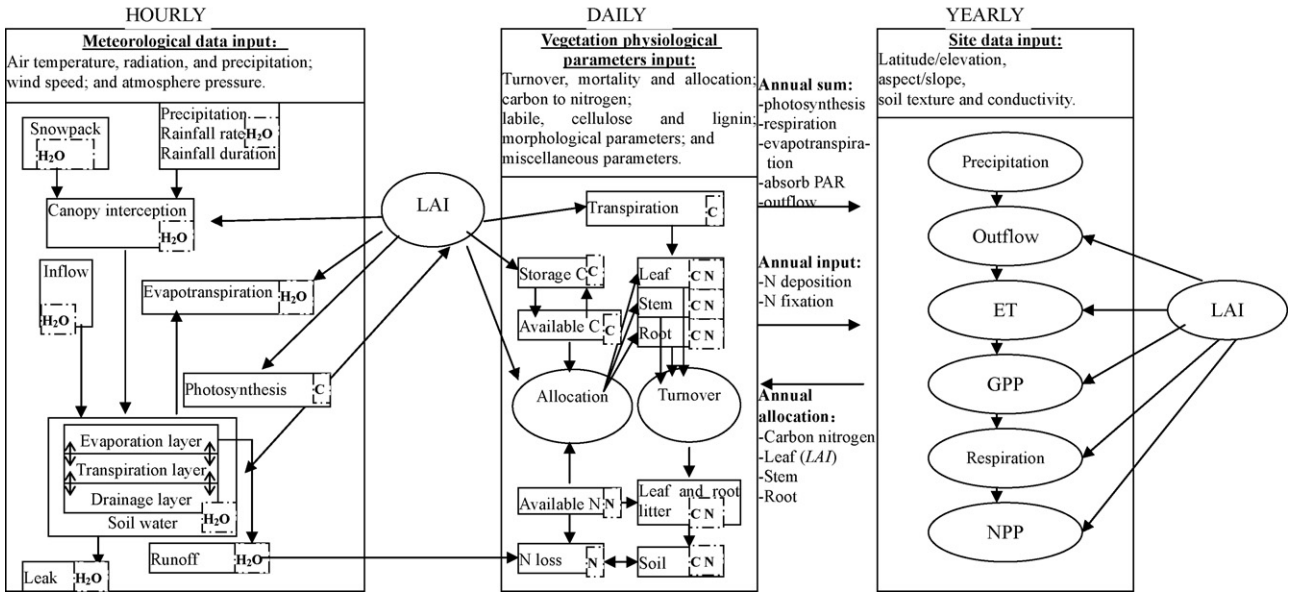

Fig. 4 – A compartment flow diagram of SWCCV, illustrating the hourly, daily and yearly components of the model. Compartments are defined by state variable number (Table 1) and by element for H_2O, water; C, carbon; and N, nitrogen.

The product of these two scalars (t_{scalar} and w_{scalar}) were summed annually and multiplied by litter and soil carbon to estimate decomposition. For soil, maximum soil carbon turnover rate was set at 0.03 per year (Academia Sinica and Ministry of Water Resources, 1993).

2.3. *Model structure*

In order to quantify the maximal vegetation production that soil water can support, we present a modeling approach integrated the physically based hydrological process and biogeochemical process. A compartment flow diagram of SWCCV, given in Fig. 4, shows combined hourly, daily and yearly cycle solution. Hydrologic balances, photosynthesis and evapotranspiration are most necessarily treated hourly because precipitation process is mostly transient in arid and semi-arid environment, and this process affect water balance immediately, and therefore photosynthesis and evapotranspiration. However, carbon allocation, litterfall and decomposition processes cannot be meaningfully calculated hourly because the minimum routinely measurable increment of these processes is typically weekly or monthly. We attempted to work at a daily step to model ecological process in great detail. Finally, the whole process is summarized at a yearly time step to sum up the annual input and annual allocation for the next year model loop. The split time resolution allows modeling processes at time scales optimum for the process dynamics.

The required variables and initial values to run SWCCV are presented in Table 1. The initialization routine is interactive, requiring input of split data and information including meteorological data, vegetation physiological parameters and site data followed the split time solution. Hydrologic variables are calculated as one-dimensional depths in meters as is common in hydrology. Stand and site conditions are also based on 1 m^2 ground area, with carbon and nitrogen variables in kg m^{-1} (Table 1). However, the model treats fluxes only in the vertical dimension, so the horizontal homogeneity is assumed for any defined area.

If soil moisture content is above the wilting point, the model produces hourly values of soil water dynamics in each of the soil layers, together with hourly values of stomatal conductance, photosynthesis, evaporation and transpiration. If required, it accumulates these values and produces at daily time step, as well as calculates LAI (total leaf area index not projected), NPP (net primary productivity), GPP (gross primary productivity) and NEE (net ecosystem exchange) dynamics. Then total NPP is converted to biomass and vegetation density follows the way given in (Luo, 1996; Ni et al., 2001). At the end of the run, a set of annual statistics for each year and, finally, a mean annual set are gathered together.

3. Model validation and use

The simulations presented here were produced by SWCCV with parameterization as described in this paper. All the parameters were obtained either from literature sources or, in the cases where there are site-specific, measurements. The model was tested using climatic conditions at Shenmu site in the north of the Loess Plateau, China, with an average annual rainfall of 437 mm (minimum 109 mm, maximum 891 mm), mean annual temperature was 8.4 °C (the coldest −9.7 °C in January, the warmest 23.7 °C in July) (Rodney et al., 2005). The natural vegetation of this region studied was *Caragana*.

Hourly meteorological data and day-length are required in the SWCCV model. Standard meteorological data included air temperature (Vaisala; HMP45A; instrument height 150 cm), humidity (Vaisala; HMP45A; 150 cm), wind speed (Young; 03001; 220 cm), precipitation (Davis Inst. Corp.; Rain Collector II), and solar radiation (Kipp and Zonen; CNR-1; 175 cm) were logged every hour at Shenmu site. Day-length is calculated by latitude and longitude.

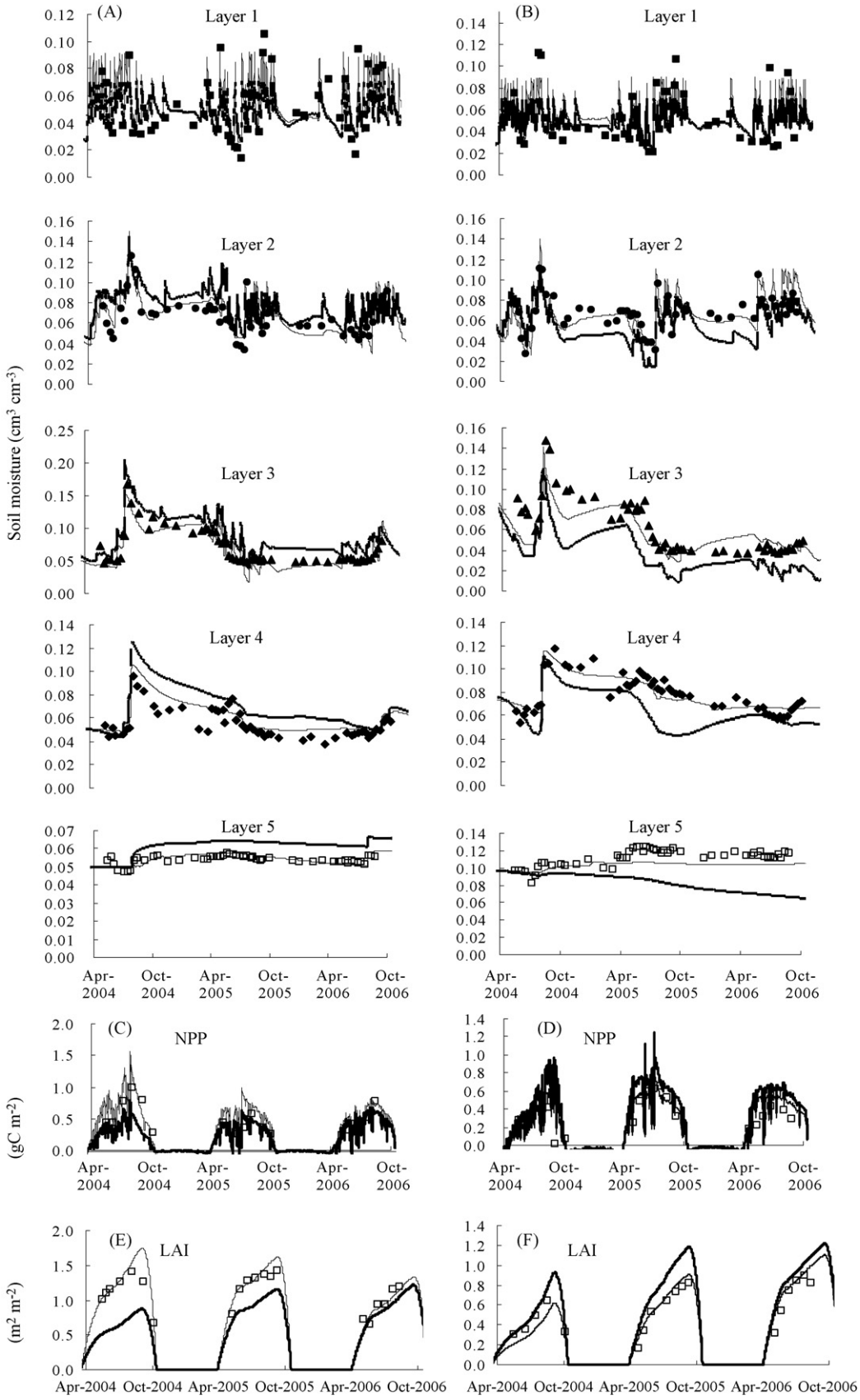

Fig. 5 – Simulated effects of current vegetation density (thin line) and soil water carrying capacity for vegetation (bold line) on soil moisture, NPP, and LAI (the symbols are values of measurements). With the average stem *C* = 0.82 kg/tree, the carrying capacity simulated is 2250 trees/hm^2 for site in right panel (6500 trees/hm^2 in current); however 6030 trees/hm^2 for site in left panel (1700 trees/hm^2 in current).

Table 2 – Correlation coefficients (R^2) between measured values and simulated values of soil moisture, NPP, and LAI at high vegetation density site and low vegetation density site, respectively

Site	Layer 1	Layer 2	Layer 3	Layer 4	Layer 5	NPP	LAI
High vegetation density	0.61	0.76	0.85	0.76	0.62	0.64	0.84
Low vegetation density	0.63	0.74	0.80	0.73	0.54	0.72	0.79

The soil texture in the experimental station is sandy loam (48% sand, 39% silt, and 13% clay), and the soil parameters and constants used in this study were shown in Table 1. The soil layer is divided as 5 layers scheme with 0.2, 0.4, 0.8, 1.5, and 3 m soil depths, respectively. Soil water data were measured by neutron probe from the surface to 600 cm (it was the vegetation rooting depths) at approximate 10 cm intervals every 10 days during plant growth period. Soil water measurements by neutron probe were found to be unreliable at this site because of low soil water contents; however, changes of soil water contents in 10-day period in each layer provided measuring accuracy of ±5% approximately.

The *Caragana* stand region consists of a 150 m × 100 m area at the site which is divided into two distinct stand density areas, each approximately 7500 m^2 in area. The higher vegetation density (HVD) is 6500 trees/hm^2 and 1700 trees/hm^2 for the lower vegetation density (LVD). We assumed that meteorological data and soil texture are uniform because the two distinct vegetation density sites are adjacent. The methodologies of forest NPP estimates followed the same ones given in Luo (1996) and Ni et al. (2001). Briefly, the forest NPP was estimated by summarizing the net increments of tree stem, branch, leaf and root. The effective leaf area index was measured using LAI2000 plant canopy analyzer (LI-COR, Inc., Lincoln, USA), and biomass measurements (fresh and dry weights) were harvested every 20 days for biomass measurements of different components (leaves and stem). The initial vegetation physiological parameters for the simulations are given in Table 1. These parameters were obtained from both published literature for these genera and observations from our previous studies.

SWCCV was developed primarily for the purpose of predicting interactions between soil water dynamics and vegetation growth under a range of forest densities. We therefore tested the accuracy which SWCCV predicted (Fig. 5, thin line) with soil moisture in each layer, LAI, and NPP observed (Fig. 5, symbols) from May, 2004 to October, 2006 for sites in the HVD (left panel, 6500 trees/hm^2) and LVD (right panel, 1700 trees/hm^2).

Ten-day means of measured and predicted θ of HVD (Fig. 5A) and LVD (Fig. 5B) are presented for each soil layer depth at two selected sites. In general, the simulated values compared well with the observed results. The largest differences between measured and simulated soil water occurs during late summer for each simulating years. The discrepancy represents either, or a combinations, of two factors: (1) the measured values are an average soil water content for the upper soil layer, and hence have statistical error in the mean. Wetting of the extreme upper profile from late-season rains is not well represented in the measured data, and total soil moisture down to subsoil may be underestimated from field data. (2) If indeed there is water loss or supply (induced by human activities or other natural factors), it is not accounted for in the model, causing simulations to inaccurately estimate recharge when vegetation is quiescent. The correlations achieved between predicted and measured soil moisture adequately meet the requirements of the expected (Table 2). But simulated soil moisture values of layer 5 is not as accurate as other layers, it is probably the vertical variability of soil texture characterized by a very heavy clay soil, requiring particular site-specific data. The low coefficients of topsoil moisture values might be the inaccurate counting of neutron probe in top soil layer. As observed, the soil moisture of the subsoil layers (for example, layer 3 and layer 4) at HVD, which dropped to the permanent wilting point in 2005 and 2006, was much lower than the same layers at LVD. In spite of the general agreements of the two sites, for a particular layer soil moisture decreased much dramatically in HVD than that in LVD from the simulation. This phenomenon was also observed in the field. The model is therefore more than adequate for calculating site feasible plant density, while still giving satisfactory predictions of soil water contents in each soil layer.

Total NPP estimates were derived from above to under ground NPP ratios reported in the literature for *Caragana* (Thornton et al., 2002). These results were compared with the same period NPP estimates derived from monthly stem-wood radial increment cores and site-specific allometric equations for *Caragana*. Test runs of the model, including sites in HVD (Fig. 5C) and in LVD (Fig. 5D), suggest that SWCCV can be applied to plant growth over a wide range of soil moisture contents of the sites.

The predicted values of LAI are good within the ranges measured for sites in HVD (Fig. 5E) and in LVD (Fig. 5F). It should be noted that the increase of LAI at lower vegetation density site is more rapid than that at in higher vegetation density site during the second and the third year because of soil moisture limits to photosynthesis.

What emerges from sensitivity runs of the model is the importance of good estimates for the permanent wilting point and field capacity in each soil layer and the initial stem carbon. The model is also sensitive to vegetation physiology parameters and the activity of the vegetation. It also requires accurate measures or estimates of meteorological data. Processes and parameter estimates which are poorly understood and require further work and specification are the effect of soil fertility, root distribute, and atmospheric CO_2 concentration.

4. Results and discussion

The objective of this modeling work was to assess the model's skill to capture soil water carrying capacity at various soil water backgrounds. The predictions of the model at HVD and LVD mentioned above, from May, 2004 to October, 2006, are also given in Fig. 5 (bold line). The number of model cycles is

8 for HVD and 6 for LVD to reach soil water carrying capacity. With the average stem C = 0.82 kg/tree, The maximum plant density simulated by SWCCV is 2250 trees/hm^2 for HVD; however 6030 trees/hm^2 for LVD when setting initial soil moisture value of simulation equal to corresponding measurements in May, 2004.

Fig. 5A and B showed modeled soil water dynamics under the maximum vegetation at two distinct soil moisture background. Soil moisture increase deeply as vegetation density fewer than the current vegetation density in HVD, and in LVD excess soil water was consumed with increasing vegetation biomass. These results suggest that HVD have overloaded the soil water carrying capacity for vegetation at present climatic scenario, and LVD can designedly plant more vegetation to maintain ecosystem developed healthy. Therefore, significant increase in vegetation density must to a great extent depend upon the local soil moisture background and climatic condition. With the increase of vegetation density, vegetation exploited more soil water in deeper soil layers at HVD than that at LVD (Fig. 5A and B). Hence, for one side, increasing vegetation density cannot only deplete the excessive soil water in the deeper soil layers, but also promote the effect of soil and water conversation. For another side, reducing vegetation density may apparently recover soil water when there are soil layers in desiccation.

The effects illustrated NPP in Fig. 5C and D are expected. For HVD (Fig. 5C), soil water content is increased by initial decreases in vegetation density, resulting in a rapid increase of NPP during the subsequent year, and therefore LAI (Fig. 5E). In contrast, predict soil water in LVD (Fig. 5B) does not decrease seriously under the predicted plant density, and NPP (Fig. 5D) and LAI (Fig. 5F) are also increased significantly with plant density in HVD. The results can happen in real.

5. Conclusions

The concept and premise of carrying-capacity are employed as tools for the operationalization of sustainable development. However, the current modeling works were limited to ensure physical or dynamical consistency of system solutions. In order to improve our understanding and quantification of soil water-vegetation interactions and soil water carrying capacity for vegetation, it is necessary to integrate hydrological and biogeochemical process model to estimate not only soil water dynamics but also its influence on vegetation density. Particular attention has been paid to the processes which strengthen or weaken the production of vegetation, including soil water affect transpiration and photosynthesis, seasonal variability of LAI feedback on soil moisture. Simulation results show that the SWCCV model, using the current climate data, vegetation physiology parameters and site-specific data, was in agreement with the soil water dynamics in each layer, as well as the variability of NPP and LAI. Then the prediction was carried out for sites in soil water in stress and soil water in abundance for Shenmu, a characteristic site of arid and semi-arid climates. The SWCCV model was successful in capturing the soil water difference between two sites in terms of controlling vegetation density. Therefore, SWCCV is a useful tool for interpreting accumulated effects of climatic and environmental conditions on management of particular vegetation systems. However, further study should be conducted, especially for various soil types and vegetations in semi-arid regions that were not addressed in the present study. Moreover, a sensitivity analysis will be further performed to capture the weight of each parameter in the model.

Acknowledgement

This work was supported by projects of China Basic Research Program and Innovation Team Program of Ministry of Education of China (2007CB106803, IRT0749) and by the Innovation Team Program of Northwest A&F University. The authors are grateful to Dr. Huo Zhu for providing soil moisture data.

REFERENCES

Academia Sinica and Ministry of Water Resources, 1993. Memoir of Northwestern Institute of Soil and Water Conservation, vol. 18. Shaanxi Scientific and Technological Press, Xian, 144 pp. (in Chinese).

Aber, J.D., Federer, C.A., 1992. A generalized, lumped-parameter model of photosynthesis, evapotranspiration and net primary production in temperate and boreal forest ecosystems. Oecologia 92, 463–474.

Andren, O., Paustian, K., 1987. Barley straw decomposition in the field:a comparison of models. Ecology 68 (5), 1190–1200.

Bosch, J.M., Hewlett, J.D., 1982. A review of catchment experiments to determine the effect of vegetation changes on water yield and evapotranspiration. J. Hydrol. 55, 3–23.

Braud, I., Vich, A.I.J., Zuluaga, J., Fornero, L., Pedrani, A., 2001. Vegetation influence on runoff and sediment yield in the Andes region: observation and modelling. J. Hydrol. 254, 124–144.

Chen, J., Liu, J., Cihlar, J., Goulden, M., 1999. Daily canopy photosynthesis model through temporal and spatial scaling for remote sensing applications. Ecol. Model. 124, 99–119.

Devonec, E., Barros, A.P., 2002. Exploring the transferability of a land surface hydrology model. J. Hydrol. 256, 258–282.

Farquhar, G.D., Von, C.C., Berry, J.A., 1980. A biochemical model of photosysthetic CO_2 assimulation in leaves of C_3 species. Planta 149, 78–99.

Garcia-Quijano, J.F., Barros, A.P., 2005. Incororating canopy physiology into a hydrological model:photosynthesis, dynamic respiration, and stomatal sensitivity. Ecol. Model. 185, 29–49.

Gardiol, J.M., Leonardo, A.S., Aida, I.D.M., 2003. Modeling evapotranspiration of corn (Zea mays) under different plant densities. J. Hydrol. 271, 291–308.

Gifford, G.F., 1976. Applicability of some infiltration formulae to rangeland infiltrometer data. J. Hydrol. 28, 1–11.

Guo, Z.S., Shao, M.A., 2004. Mathematical model for determining vegetation carrying capacity of soil water. J. Hydr. Eng. 10, 95–99 (in Chinese with English Abstract).

Jamieson, P.D., Ewert, F., 1999. The role of roots in controlling soil water extraction during drought: an analysis by simulation. Field Crops Res. 60, 267–280.

Khanna, P., Ram Babu, P., Suju George, M., 1999. Carrying-capacity as a basis for sustainable development: A case study of National Capital Region in India. Prog. Plann. 52 (1), 101–166.

Kyushik, O., Yeunwoo, J., Dongkun, L., Wangkey, L., Jaeyong, C., 2005. Determining development density using the Urban Carrying Capacity Assessment System. Landscape Urban Plann. 73, 1–15.

Laio, F., Porporato, A., Ridolfi, L., Rodriguez-Iturbe, I., 2001. Plants in water-controlled ecosystems: active role in hydrologic processes and response to water stress: II. Probabilistic soil moisture dynamics. Adv. Water Resour. 24 (7), 707.

Li, K.Y., De Jong, R., Boisvert, J.B., 2001. An exponential root-water-uptake model with water stress compensation. J. Hydrol. 252, 189–204.

Lloyd, J., Taylor, J.A., 1994. On the temperature dependence of soil respiration. Funct. Ecol. 8, 315–323.

Luo, T.X., 1996. Patters of Net Primary Productivity for Chinese Major Dorest Types and their Mathematical Models. Commission for Comprehensive Survey of Natural Resources, Chinese Academy of Science, Beijing, 211 pp.

Maidment, D.R., 1993. Handbook of Hydrology. McGraw Hill, New York.

Molz, F.J., Remson, I., 1970. Extraction term models of soil moisture use by transpiring plants. Water Resour. Res. 6, 1346–1356.

Monteith, J.L., 1965. Evaporation and environment. Proc. Soc. Exp. Biol. 19, 205–234.

Ni, J., Zhang, X.S., Scurlock, J.M.O., 2001. Synthesis and analysis of biomass and net primary productivity in Chinese forests. Ann. Forest Sci. 58, 351–384.

Orchard, V.A., Cook, F.J., 1983. Relationship between soil respiration and soil moisture. Soil Biol. Biochem. 15 (4), 447–453.

Parton, W.A., et al., 1996. Generalized model for N_2 and N_2O production from nitrification and denitrification. Global Biogeochem. Cycle 10, 401–412.

Raich, J.W., et al., 1991. Potential net primary productivity in South America: application of a global model. Ecol. Appl. 1, 399–429.

Rodney, E.W., Nikhil, V.N., Barry, D.S., Robert, O.T., 2005. Effects of planting density on canopy dynamics and stem growth for intensively managed loblolly pine stands. Forest Ecol. Manag. 205, 29–41.

Running, S., Nemani, R., Hungerfored, R., 1987. Extrapolation of synoptic meteorological data in mountainous terrain and its use for simulating forest evapotranspiration and photosynthesis. Can. J. For. Res. 17, 472–483.

Running, S.W., Gower, S.T., 1991. FOREST-BGC, a general model of forest ecosystem processes for application. II. Dynamic carbon allocation and nitrogen budgets. Tree Physiol. 9, 147–160.

Ryan, M.G., 1991. Effects of climate change on plant respiration. Ecol. Appl. 1, 157–167.

Schneider, D. M., Godschalk, D.R., Axler, N., 1978. The carrying capacity concept as a planning tool. Planning Advisory Service Report Thesis, Chicago, 338 pp.

Schulze, D., 1986. Carbon dioxide and water vapor exchange in response to drought in the atmosphere and in the soil. Annu. Rev. Plant Physiol. 37, 247–274.

Shuttleworth, W.J., Wallace, J.S., 1985. Evaporation from sparse crops-an energy combination theory. Quart. J. R. Meteor. Soc. 111, 839–855.

Tague, C.L., Band, L.E., 2004. RHESSys: Regional Hydro-Ecologic Simulation System—An object-oriented approach to spatially distributed modeling of carbon, water, and nutrient cycling. Earth Interact. 8, 1–42.

Thornton, P.E., Law, B.E., Gholz, H.L., Clark, K.L., Falge, E., Ellsworth, D.S., Goldstein, A.H., Monson, R.K., Hollinger, D., Falk, M., 2002. Modeling and measuring the effects of disturbance history and climate on carbon and water budgets in evergreen needleleaf forests. Agric. Forest Meteorol. 113, 185–222.

Townsend, A.R., Vitousek, P.M., Trumbore, S.E., 1995. Soil organic matter dynamics along gradients in temperature and land use on the island of Hawaii. Ecology 76, 721–733.

van Dijk, A.I.J.M., Bruijnzeel, L.A., 2003. Terrace erosion and sediment transport model: a new tool for soil conservation planning in bench-terraced steeplands. Environ. Modell. Softw. 18, 839–850.

Vörösmarty, C.J., et al., 1989. Continental scale models of water balance and fluvial transport: an application to South America. Global Biogeochem. Cycle 3, 241–265.

Wang, X.L., Cai, Q.G., 1999. Reasons and profits analysis of how the vegetation measure controls slopeland soil erosion. Arid Zone Res. 16, 37–42 (in Chinese with English Abstract).

White, M.A., Thornton, P.E., Running, S.W., Nemani, R.R., 2000. Parameterization and sensitivity analysis of the "BIOME-BGC" terrestrial ecosystem model: net primary production controls. Earth Interact. 4 (3), 1–15.

Yu, X.X., Zhang, X.X., Li, J.L., Zhang, M.L., Xie, Y.Y., 2006. Effects of vegetation cover and precipitation on the process of sediment produced by erosion in a small watershed of loess region. Acta Ecologica Sinica 26 (1), 1–8.

Zeide, B., 2004. Optimal Stand density: a solution. Can. J. Forest Res. 34 (4), 846–854.

Zhou, Z.C., Shangguan, Z.P., Zhao, D., 2006. Modeling vegetation coverage and soil erosion in the Loess Plateau area of China. Ecol. Model 198, 263–268.